

SATGround : A Spatially-Aware Approach for Visual Grounding in Remote Sensing

Aysim Toker¹, Andreea-Maria Oncescu¹, Roy Miles¹, Ismail Elezi¹, and Jiankang Deng²

¹ Huawei London Research Center

² Imperial College London

Abstract. Vision-language models (VLMs) are emerging as powerful generalist tools for remote sensing, capable of integrating information across diverse tasks and enabling flexible, instruction-based interactions via a chat interface. In this work, we enhance VLM-based visual grounding in satellite imagery by proposing a novel structured localization mechanism. Our approach involves finetuning a pretrained VLM on a diverse set of instruction-following tasks, while interfacing a dedicated grounding module through specialized control tokens for localization. This method facilitates joint reasoning over both language and spatial information, significantly enhancing the model’s ability to precisely localize objects in complex satellite scenes. We evaluate our framework on several remote sensing benchmarks, consistently improving the state-of-the-art, including a 33.2% relative improvement over previous methods on visual grounding. Our results highlight the benefits of integrating structured spatial reasoning into VLMs, paving the way for more reliable real-world satellite data analysis. Code will be released upon acceptance.

1 Introduction

The rapid proliferation of Earth observation technologies in recent years has provided unprecedented access to high-resolution satellite imagery, enabling advanced monitoring and analysis of the Earth’s surface. Extracting actionable insights from this vast data depends on scalable machine learning approaches. Open data initiatives like Landsat [60] and Copernicus [4] have facilitated the curation of specialized datasets for a wide range of applications, including disaster response, food security, and urban growth analysis. These applications require models capable of performing complex tasks, such as object recognition, temporal change detection, and interpreting scene compositionality.

Traditional machine learning approaches tackle these challenges by defining discriminative models for specific tasks such as scene classification or semantic segmentation. More recently, vision-language models (VLMs) have opened up promising new applications for multi-modal satellite data. The advantage of such generalist models lies in large-scale pretraining on image-text pairs and fine-tuning on instructional prompts. Hence, they can leverage prior knowledge about



Fig. 1: We propose a novel spatially-aware grounding mechanism for vision-language models (VLMs) in remote sensing. Our approach (green) integrates structured spatial information, leading to significantly improved localization capabilities compared to methods that treat bounding boxes as text. The qualitative examples shown here highlight our model’s superior alignment with the ground truth (red) on diverse user prompts, outperforming state-of-the-art baselines InternVL [12], CVPR’24 (orange), and EarthDial [51], CVPR’25 (yellow).

real-world scenes and reason about their content in a dialogue-based format, allowing them to respond to complex user queries. This conversational paradigm, where users issue queries and AI assistants generate responses, enables the joint learning of linguistic and visual semantics. A key question is how we can ensure natural interaction with these models while obtaining precise and accurate information about a given satellite scene.

One common approach is visual grounding for detection, which reinforces the link between textual descriptions of objects and their corresponding visual representation. Following the pioneering approach GeoChat [26], a number of recent works aim to leverage visual grounding for remote sensing tasks through bounding box detection [39, 40, 51, 68]. A common strategy in these approaches is embedding bounding box locations into the prompt by converting them into text form, which may also require assigning special tokens for each possible numeric value. This is straightforward and convenient for interfacing off-the-shelf vision-language models, but it also has significant limitations due to the lack of geometric structure associated with such numerical tokens [48–50]. Without an explicit spatial metric, the model does not have a notion of proximity, decreasing its robustness to small perturbations and out-of-distribution generalization. We show that this can inhibit the localization performance in practice, indicating a demand for more specialized grounding approaches.

In this work, we introduce *SATGround*, a novel grounding technique for vision-language models that integrates multi-modal learning with a specialized localization mechanism for remote sensing data. We adapt existing instruction-following datasets by introducing special tokens which act as anchors for bounding box prediction and localization. Rather than converting bounding boxes into a text representation, our LLM decoder operates simultaneously in language space and bounding box space. This dual approach combines visual and textual semantics while facilitating communication between these two modalities.

SATGround is a generalist framework that can be adapted to different remote sensing applications, making it both scalable and highly flexible. Our structured visual grounding technique bridges the gap between language and spatial reasoning, thus improving the localization robustness and consistency across diverse

satellite imagery datasets compared to existing grounding approaches. In summary, our **contributions** are the following:

- We **propose** *SATGround*, a novel, spatially-aware localization technique of visual grounding for Earth observation data.
- We **finetune** an existing generalist vision-language model for both language and detection objectives, interfacing these two modalities via special control tokens and a custom localization module.
- We **advance** the state-of-the-art on several remote sensing benchmarks [14, 21, 26, 36, 51], achieving a significant relative improvement of 33.2% in visual grounding performance compared to existing methods.

2 Related work

Vision-language models. Over the last few years, multi-modal learning for vision tasks has become an extensively studied topic, with various approaches and applications. We provide an overview of techniques most relevant to our work here and refer to a recent survey [71] for a more comprehensive review.

Early multi-modal approaches [25, 37, 45, 62, 64, 67] revolve around a common paradigm where, given large-scale text-image pairs [8, 47], the model aims to integrate features into a joint embedding space with techniques such as contrastive learning. Once the embeddings are learned, this shared space is then leveraged for zero-shot learning across a variety of tasks, such as classification [45, 67], retrieval [17, 32, 43, 57], object detection [3, 32]. Later, numerous extensions were proposed that apply such models to open-vocabulary detection [16, 18, 20, 38], segmentation [55, 56, 61], or 3D open-world learning [72, 77]. These methods focus on pretraining base models and thus require finetuning for discriminative tasks.

More recently, models like LLaVA [34] and GPT-4 [1, 75] have introduced assistants capable of processing multi-modal inputs, as well as generating task-specific outputs. LLaVA [34] provides a general framework that combines language instructions and visual embeddings into a single sequence, enabling the use of a pretrained LLM [15, 19, 41, 54, 58] as a decoder. In this work, we adopt a similar strategy, leveraging a pretrained LLM as a decoder to ground a vision-language model for Earth observation tasks.

Grounding vision-language models. The goal of visual grounding for localization is to improve the ability of models to identify the location of objects based on text-based queries. Training a VLM typically consists of two stages: a pretraining stage and a visual instruction tuning stage. Several works have proposed to integrate grounding into this second stage by embedding location information into a text representation [11, 42, 59, 63]. This has led to many refined instruction tuning datasets [11, 29, 42, 69] with a focus on referring and grounding tasks. However, a common limitation of all models trained in this way is that they lack any explicit geometric modeling and are contingent on the model’s ability to interpret text-based location information. Prior work has shown [48–50] that language models often struggle with numerical inference tasks

and spatial understanding due to challenges arising from default tokenization, positional encoding schemes, and limitations in multi-step reasoning.

A number of works [28, 35, 70, 74] attempted to address this problem by proposing more specialized grounding modules. Unfortunately, these techniques are often highly engineered and specific to common object-centric data [32]. In contrast, we propose a simple new grounding technique for remote sensing data – interfacing a generalist VLM via specialized task tokens and leveraging its rich visual semantic features to predict bounding box coordinates.

Vision-language models for satellite imagery. Applying existing VLMs to Earth observation tasks presents a unique set of challenges, as the large domain gap between satellite and natural images often limits their performance on remote sensing data. For an overview of recent works aimed at adapting general multi-modal methods for satellite tasks, we refer to the recent survey by Li et al. [30]. Such approaches leverage task-specific datasets to enhance performance in zero-shot classification [31, 44], image captioning [78], and visual question answering [6, 9, 65]. However, these models are typically limited to specific tasks and lack the ability to engage in instruction-following dialogues.

The pioneering work RSGPT [23] introduces the RSICap dataset to fine-tune multi-modal models for instruction-following capabilities on remote sensing data, with applications such as image captioning and visual question answering (VQA). More recently, GeoChat [26] proposed to adapt the LLaVA [34] model to remote sensing data, while integrating special task tokens into the textual instructions. This improves the zero-shot performance across a broad set of tasks, including image and region captioning, VQA, scene classification, and grounding descriptions. Following this trend, similar approaches such as SkyEyeGPT [68], LHRS-Bot [39], and VHM [40] employ comparable instruction-following architectures. The most recent efforts, such as EarthGPT [73] and EarthDial [51], introduce multi-modal models and datasets that fuse multiple data forms, such as optical, SAR, and multi-spectral.

While these works show the promise of grounded conversation in remote sensing, they often struggle to ground objects due to their reliance on encoding location context into text. In our work, we address this limitation by introducing a dual approach that jointly models both language and bounding box spaces, enabling more precise and interpretable grounding in remote sensing data.

3 Method

3.1 Problem formulation

The basic framework for grounded multi-modal learning on Earth observation data can be specified as follows:

$$\mathcal{M}_{\text{vlm}} : (\mathbf{x}, \mathbf{q}) \mapsto \mathbf{a}, \quad (1)$$

where the vision-language model \mathcal{M}_{vlm} processes a satellite image $\mathbf{x} \in \mathbb{R}^{H \times W \times 3}$ and a text query $\mathbf{q} \in \mathcal{V}^{N_q}$ to produce a textual response $\mathbf{a} \in \mathcal{V}^{N_a}$. We commonly

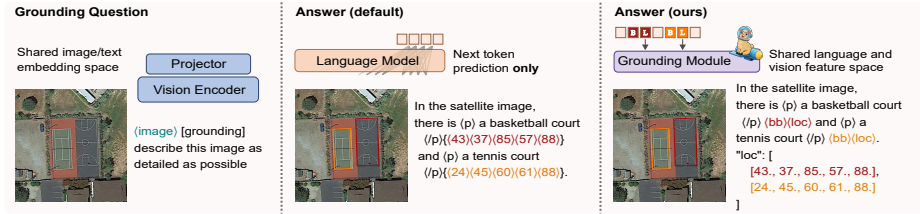


Fig. 2: Structured visual grounding. For a given user query (left), we visualize the conventional text-based visual grounding approach (middle), compared to our structured explicit grounding format (right). For illustration purposes, we show the ground-truth bounding box location values (red and orange) in both cases. Instead of returning bounding box coordinates as text, we model a dedicated localization mechanism interfaced by special control tokens $\langle bb \rangle$ and $\langle loc \rangle$, see Sec. 3.2 for more details.

assume that addressing \mathbf{q} requires reasoning about the content of the image \mathbf{x} . Here, $W, H \in \mathbb{N}$ denote the spatial size of the input image, while $N_q, N_a \in \mathbb{N}$ correspond to the sequence length of \mathbf{q} and \mathbf{a} , respectively. Both sequences specify tokens from a common vocabulary:

$$\mathcal{V} := \mathcal{T} \cup \mathcal{S} := \{\mathbf{t}_1, \dots, \mathbf{t}_{|\mathcal{T}|}\} \cup \{\langle bos \rangle, \langle eos \rangle, \langle pad \rangle\}, \quad (2)$$

which comprises text tokens \mathcal{T} , as well as special control tokens \mathcal{S} , such as the beginning-of-sequence token $\langle bos \rangle$, the end-of-sequence token $\langle eos \rangle$, and the padding token $\langle pad \rangle$.

Motivation. Standard grounding techniques for vision-language models on Earth observation data embed location context within text representations, to allow implicit learning of spatial relations through next-token prediction. However, this method lacks explicit geometric modeling, which hinders the ability of the model to capture the precise spatial layout of satellite images.

To address this limitation, we modify the framework to incorporate explicit geometric reasoning. Rather than relying on implicit location information via next-token prediction, we introduce a grounding mechanism to predict bounding box locations directly. This model is defined as follows:

$$\mathcal{M}_{loc} : (\mathbf{x}, \mathbf{q}) \mapsto (\mathbf{a}, \ell). \quad (3)$$

Besides mapping an image $\mathbf{x} \in \mathbb{R}^{H \times W \times 3}$ and text query $\mathbf{q} \in \bar{\mathcal{V}}^{N_q}$ to a reply $\mathbf{a} \in \bar{\mathcal{V}}^{N_a}$, this localization model \mathcal{M}_{loc} also directly predicts the bounding box locations $\ell \in \mathbb{R}^{L \times 5}$. Here, ℓ represents coordinates of $L \in \mathbb{N}$ different predicted bounding boxes, see Sec. 3.3 for bounding box specifications. We further append two additional special tokens to the vocabulary:

$$\bar{\mathcal{V}} := \mathcal{V} \cup \{\langle bb \rangle, \langle loc \rangle\}, \quad (4)$$

denoting bounding boxes $\langle bb \rangle$ and location $\langle loc \rangle$ tokens, respectively. In Fig. 2, we visualize our bounding box representation for a given query in comparison to the standard text-based format. We describe in Sec. 3.2 how integrating these tokens enables structured visual grounding in our model.

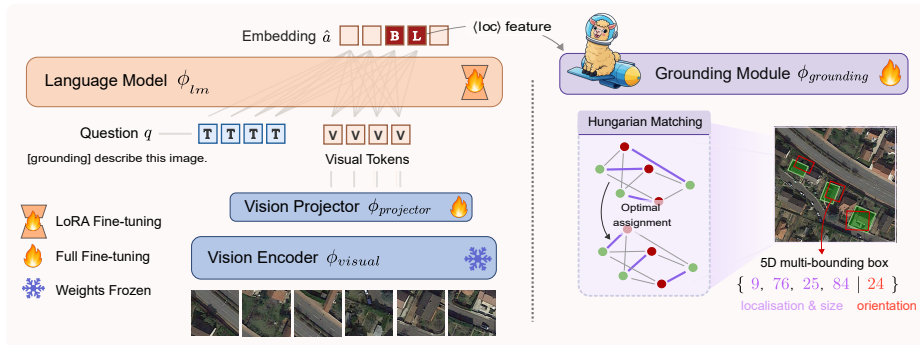


Fig. 3: Method overview. We summarize the different components of our model. Visual inputs are encoded using a frozen vision backbone, ϕ_{visual} , and a trainable adapter $\phi_{projector}$. The extracted vision tokens are then concatenated with the user query and passed to the language model ϕ_{lm} based on LLaVA [34], which we finetune by applying LoRA [22]. The model’s response contains both standard text tokens and occasional $\langle bb \rangle$ and $\langle loc \rangle$ tokens, see Sec. 3.2 for more details. Any resulting $\langle loc \rangle$ feature embeddings are passed to the grounding module $\phi_{grounding}$ which produces the final bounding box predictions and matches them by using the Hungarian algorithm.

To facilitate gradient-based learning, we define \mathcal{M}_{loc} with a differentiable mapping from image $\hat{\mathbf{x}}$ and text $\hat{\mathbf{q}}$ embeddings to locations ℓ . By convention, we denote $\hat{\mathbf{x}}$ and $\hat{\mathbf{q}}$ for the embedded features in latent space corresponding to data instances such as images \mathbf{x} and text \mathbf{q} . The model thus optimizes the language output and bounding box locations simultaneously, enabling it to reason about how geometric details correspond to textual cues.

3.2 Structured visual grounding

The vocabulary space of possible output tokens in Eq. (4) includes text tokens, control tokens ($\langle bos \rangle$, $\langle eos \rangle$, $\langle pad \rangle$), and two additional special tokens $\langle bb \rangle$ and $\langle loc \rangle$. We now detail the latter two, which specify a grounding interface for regressing bounding box parameters in our model. Instead of forcing the language model to output numerical coordinates as raw text, this interface routes spatial predictions to a dedicated grounding module.

Bounding box and location tokens. By convention, the two special bounding box tokens always appear in sequence $\langle bb \rangle \langle loc \rangle$ in a given text sample. They serve two distinct purposes: $\langle bb \rangle$ indicates that the model produces a bounding box as part of the current predicted sentence. $\langle loc \rangle$ then provides latent features for the corresponding bounding box parameters (*i.e.*, its location and orientation). The design choice of introducing two separate tokens $\langle bb \rangle$ and $\langle loc \rangle$ ensures a clear separation of responsibilities, and avoids sharing the capacity of a single embedding vector between these tasks. Our ablation study in Tab. 5(a) confirms this design is crucial, demonstrating that the separated tokens achieve an improved performance compared to a single-token approach.

Training. During training, our model naturally produces bounding box tokens $\mathbf{a}_t = \langle bb \rangle$ as part of the output sequence $\mathbf{a} \in \bar{\mathcal{V}}^{N_a}$ via standard next-token prediction. In contrast, the location tokens $\langle loc \rangle$ are masked out when computing the cross-entropy token loss, analogous to padding tokens $\langle pad \rangle$. Since $\langle loc \rangle$ always appears right after $\langle bb \rangle$ in a fully deterministic manner, it carries no information for next-token prediction (zero entropy). Instead, we simply pass the latent embeddings $\hat{\mathbf{a}}_t \in \mathbb{R}^D$ associated with the $\mathbf{a}_t = \langle loc \rangle$ tokens to our grounding module $\phi_{\text{grounding}}$, where D denotes the embedding dimensionality. This separate head is responsible for regressing the final bounding box coordinates:

$$\phi_{\text{grounding}} : \begin{cases} \mathbb{R}^{L \times D} \rightarrow \mathbb{R}^{L \times 5} \\ \{\hat{\mathbf{a}}_t \in \mathbb{R}^D \mid \mathbf{a}_t = \langle loc \rangle\} \mapsto \boldsymbol{\ell} \end{cases} \quad (5)$$

where $\boldsymbol{\ell} \in \mathbb{R}^{L \times 5}$ denotes the predicted bounding box coordinates. In practice, $\phi_{\text{grounding}}$ is parameterized as a shallow MLP. The primary goal is to accurately predict the location of a specific object while interfacing the VLM’s language capabilities. We provide a comprehensive graphical representation of our approach in Fig. 3. To finetune the model, we optimize for both the language modeling and location tasks simultaneously:

$$\mathcal{L} = \lambda_{\text{text}} \mathcal{L}_{\text{CE}} + \lambda_{\text{bb}} \mathcal{L}_{\text{ground}}, \quad (6)$$

where \mathcal{L}_{CE} represents the cross-entropy loss for predicting the next token in the sequence, $\mathcal{L}_{\text{ground}}$ is the grounding loss for regressing the bounding box coordinates, and $\lambda_{\text{text}}, \lambda_{\text{bb}}$ are hyperparameters indicating their relative weights. **Bipartite matching.** Since the model may output bounding box predictions for multiple distinct visual categories in a single response, a standard global, class-agnostic bipartite matching can lead to semantically flawed assignments. For instance, in the scenario depicted in Fig. 2, the model might match a “basketball court” prediction to a “tennis court” annotation solely due to spatial proximity. To enforce permutation invariance while preserving semantic associations, we partition the predicted bounding boxes into G distinct referring expression groups based on their sequential adjacency within the generated text, specifically consecutive $\langle bb \rangle$ tokens uninterrupted by descriptive text. Within each group, we compute a bipartite matching of the predicted bounding boxes $\boldsymbol{\ell} \in \mathbb{R}^{L \times 5}$ to the reference bounding box coordinates $\mathbf{k} \in \mathbb{R}^{K \times 5}$ to calculate the grounding loss $\mathcal{L}_{\text{ground}}$. Following standard practice in the literature [7, 52], this is formulated as a linear sum assignment:

$$\mathcal{L}_{\text{ground}}(\boldsymbol{\ell}, \mathbf{k}) := \sum_{g=1}^G \min_{\rho^{(g)} \in \mathcal{P}_{L_g, K_g}} \sum_{i=1}^{L_g} \sum_{j=1}^{K_g} \rho_{i,j}^{(g)} \|\boldsymbol{\ell}_i^{(g)} - \mathbf{k}_j^{(g)}\|_1 \quad (7)$$

which can be efficiently solved using the Hungarian algorithm [27]. Here, $\rho^{(g)} \in \mathcal{P}_{L_g, K_g} \subset \{0, 1\}^{L_g \times K_g}$ denotes a partial permutation matrix that defines an optimal one-to-one matching between a subset of the predicted and reference boxes within group g , allowing for unmatched predictions or ground-truth boxes

when their counts differ. By resolving assignment ambiguities strictly among bounding boxes referring to the same visual entity, this local formulation effectively eliminates cross-expression contamination. As demonstrated in our ablation studies (Tab. 5(a)), enforcing this grouped, permutation-invariant matching is crucial for preventing semantic mismatches and maintaining precise localization. By isolating this spatial reasoning within a dedicated module, the primary text generation of the VLM remains unhindered and highly efficient.

Inference. During inference, we apply standard next-token prediction in a greedy sampling scheme to obtain an answer sequence $\mathbf{a} \in \mathcal{V}^{N_a}$ and bounding box coordinates $\ell \in \mathbb{R}^{L \times 5}$ from the model for a given query sequence $\mathbf{q} \in \mathcal{V}^{N_q}$ and reference image $\mathbf{x} \in \mathbb{R}^{H \times W \times 3}$. Whenever the model produces a $\langle bb \rangle$ token, we do not query the LLM and instead append a $\langle loc \rangle$ token immediately afterwards in a fully deterministic manner. We further register any such occurrences of $\langle loc \rangle$ tokens and use the resulting features to query our grounding module $\phi_{\text{grounding}}$ at the very end. Algorithm 1 details this sampling procedure.

Algorithm 1 Greedy sampling. Pseudocode for greedy sampling in our model. The model’s LM head $\phi_{\text{lm-head}}$ selects the most probable token at each step without randomness. After all answer tokens are generated, we additionally query the grounding module $\phi_{\text{grounding}}$ to predict a set of bounding box parameters for each instance of a predicted location token $\mathbf{a}_t = \langle loc \rangle$.

Input: Image $\mathbf{x} \in \mathbb{R}^{H \times W \times 3}$, query $\mathbf{q} \in \mathcal{V}^{N_q}$
Returns: Answer tokens $(\mathbf{a}_1, \dots, \mathbf{a}_{N_a}) \in \mathcal{V}^{N_a}$,
 bounding box parameters $\ell \in \mathbb{R}^{L \times 5}$

- 1: // Compute visual $\hat{\mathbf{x}}$ and textual $\hat{\mathbf{q}}$ embeddings:
 $\hat{\mathbf{x}} \leftarrow \phi_{\text{projector}} \circ \phi_{\text{visual}}(\mathbf{x}) \in \mathbb{R}^{P \times D}$; $\hat{\mathbf{q}} \leftarrow \phi_{\text{embed}}(\mathbf{q}) \in \mathbb{R}^{N_q \times D}$; $\mathbf{a}_0 \leftarrow \emptyset$
- 2: **for** $t = 1$ to N_a **do** // Iteratively generate tokens
- 3: **if** $\mathbf{a}_{t-1} = \langle eos \rangle$ **then**
- 4: **Break** // Stop generation after EOS
- 5: **else if** $\mathbf{a}_{t-1} = \langle bb \rangle$ **then**
 $\mathbf{a}_t \leftarrow \langle loc \rangle$ // Deterministic $\langle loc \rangle$ after $\langle bb \rangle$ token
- 6: **else**
 $\hat{\mathbf{a}}_t \leftarrow \phi_{\text{lm}}(\hat{\mathbf{x}}, \hat{\mathbf{q}} | \mathbf{a}_{:t})$ // Query next token from the LM
 $\mathbf{a}_t \leftarrow \phi_{\text{lm-head}}(\hat{\mathbf{a}}_t) \in \bar{\mathcal{V}}$ // Apply LM head
- 7: **end if**
- 8: **end for**
 $\hat{\mathbf{a}}_{\text{loc}} \leftarrow \{\hat{\mathbf{a}}_t \in \mathbb{R}^D | \mathbf{a}_t = \langle loc \rangle\} \in \mathbb{R}^{L \times D}$ // Extract location tokens
 $\ell \leftarrow \phi_{\text{grounding}}(\hat{\mathbf{a}}_{\text{loc}})$ // Query grounding module
- 9: **return** \mathbf{a}, ℓ

3.3 Implementation details

Oriented bounding box representation. Unlike natural images, objects in satellite imagery can appear at arbitrary orientations due to the overhead viewing angle, making axis-aligned bounding boxes a poor fit. We therefore model oriented bounding boxes (OBBs) to capture both the spatial extent and the rotation of each object. Concretely, each bounding box is parameterized as

a 5-tuple $(x_1, y_1, x_2, y_2, \theta)$, where (x_1, y_1) and (x_2, y_2) denote the top-left and bottom-right corners, and $\theta \in [0^\circ, 180^\circ)$ specifies the counter-clockwise rotation from the horizontal axis. Following the annotation convention of GeoChat [26] and EarthDial [51], coordinates and angles in the dataset are normalized to $[0, 100]$ via explicit linear mapping: $x_{norm} = 100 \cdot x/W$, $y_{norm} = 100 \cdot y/H$, and $\theta_{norm} = 100 \cdot \theta/180^\circ$. For training, we further rescale these values to continuous targets in $[0, 1]$. To ensure the output predictions from $\phi_{\text{grounding}}$ strictly adhere to this valid range, we apply a sigmoid activation function to the final layer. We ablate this design choice against unconstrained linear outputs in Tab. 5(d); while both configurations perform reasonably, the sigmoid-constrained head yields consistently higher accuracy across all metrics.

Architecture details. Our model’s core architecture consists of a pretrained, frozen ViT visual encoder [45], a trainable vision projector, and a language decoder. We also employ a grounding module ($\phi_{\text{grounding}}$) consisting of a 2-layer MLP, which is responsible for mapping our location embeddings ($\hat{\mathbf{a}}_t \in \mathbb{R}^D$ associated with $\mathbf{a}_t = \langle loc \rangle$) to bounding box coordinates, as detailed in Sec. 3.2. To ensure a fair comparison with the GeoChat and EarthDial baseline approaches, our experiments use the same respective language decoder. Specifically, we use the Vicuna-v1.5 [15] model for the GeoChat comparison and the Phi-3-mini [2] model for EarthDial. For data processing on GeoChat, we use 504×504 image inputs with interpolated positional embeddings. For the EarthDial benchmark, we employ the multi-modal (i.e., multi-spectral, SAR, temporal) and multi-resolution data fusion strategy detailed in [51]. Unless stated otherwise, all following experiments use this EarthDial setting.

Training details. To develop a generalist model capable of diverse remote sensing tasks, we finetune on the GeoChat [26] and EarthDial [51] datasets. These provide a diverse suite of tasks, including VQA, grounding, region captioning, and scene classification, aggregated from multiple sources [13, 36, 46]. We finetune our model for 1 epoch with a batch size of 16, using the AdamW optimizer with a learning rate of 2×10^{-4} and a cosine annealing schedule. To keep the finetuning lightweight, we apply LoRA [22] with rank $r = 64$ and scaling factor $\alpha = 16$ on the language backbone, while keeping the vision encoder frozen. The grounding module $\phi_{\text{grounding}}$ and the vision-language projector are trained with half precision. Our total trainable overhead amounts to only 16.8M parameters.

4 Experiments

We evaluate our method on several tasks, including referring expression detection, grounding description, and two visual question answering benchmarks. For several of these tasks, we also assess generalization to different datasets in a zero-shot manner.

4.1 Grounding and referring expression detection

Dataset. We evaluate our model on the GeoChat [26] test set, and further assess zero-shot performance on NWPU VHR-10 [14], Swimming Pool [51] and Urban

Table 1: Quantitative results for visual grounding and referring on the GeoChat benchmark. We report the accuracy (%) score. Performance is broken down by object size (Small, Medium, Large) and task type. For the Grounding and Referring tasks, we evaluate performance on prompts with single vs. multiple objects. The Avg. column shows the mean score for each task category.

Model	Object Size			Grounding			Referring			Overall
	Small	Medium	Large	Single	Multi	Avg.	Single	Multi	Avg.	
<i>Finetuned on GeoChat</i>										
LHRs-Bot [39]	0.2	1.9	9.4	18.6	3.8	5.2	3.2	1.2	2.5	2.7
MiniGPTv2 [10]	1.7	9.9	21.9	9.1	3.6	2.6	-	-	8.2	7.6
GeoChat [26]	2.9	13.6	21.7	16.0	4.3	11.8	-	-	10.5	10.6
TeoChat [24]	2.3	11.6	29.0	32.2	9.3	10.6	15.1	4.8	11.2	11.1
InternVL2-4B [12]	7.0	22.3	33.5	24.4	11.5	12.5	25.6	8.4	18.9	18.2
EarthDial [51]	6.8	23.8	32.9	25.9	13.0	13.9	26.0	8.4	19.3	18.6
Ours	10.1	29.2	44.5	39.0	18.7	20.2	33.8	9.0	24.8	24.4
<i>Finetuned on EarthDial</i>										
EarthDial [51]	11.4	31.7	39.1	28.2	18.1	18.8	34.4	12.0	25.8	25.0
Ours	13.5	39.5	57.9	38.7	29.7	30.9	38.8	15.9	33.4	33.3

Tree Crown Detection [66]. These four datasets comprise 7,593, 1,601, 5,697, and 1,279 instances, respectively, all of which feature a mix of single and multi-object queries. The benchmarks differ in their task definition: by design, GeoChat categorizes queries into distinct “Grounding” and “Referring” groups based on object attributes, while the remaining three benchmarks feature a single, holistic “Referring” task. This diverse selection of datasets ensures our model is rigorously tested across a wide variety of object distributions and scales.

Task. The objective here is to precisely localize the visual objects specified by a text query \mathbf{q} within an input image \mathbf{x} , outputting their corresponding bounding box locations ℓ . The queries in the considered benchmarks refer to diverse objects of interest, including storage tanks, cars, and airplanes, swimming pools, as well as larger objects such as football fields and bridges. We follow the prior convention [26, 51] of reporting the acc@0.5 metric as the main evaluation score, defined as the fraction of correct predictions with an IoU score larger than 0.5.

Discussion. We report quantitative results on the GeoChat test set in Tab. 1. The table details two finetuning experiments. In both cases, our method demonstrates clear performance gains: on the GeoChat dataset, we achieve 24.4% accuracy, outperforming the strongest baseline EarthDial by 5.8%. When finetuning on the EarthDial dataset, our model improves the overall accuracy by a sizable margin of 8.3% (relative improvement of 33.2%). This robust performance further translates to the zero-shot setting shown in Tab. 2, where our model outperforms baseline methods on two out of three considered downstream tasks (NWPU VHR-10 and Swimming Pools), while remaining competitive on Tree Crown Detection. We further provide several qualitative examples in Fig. 4.

4.2 Grounding description

Datasets. We evaluate the grounding description capabilities of our model in a zero-shot setting on four benchmarks: HIT-UAV [53], NWPU VHR-10 [14],

Table 2: Quantitative results for zero-shot referring object detection. We compare our model’s generalization performance against several baselines on three datasets: NWPU VHR-10 [14], Swimming Pool [51], and Urban Tree Crown Detection [66].

Model	NWPU VHR-10 [14]					Swimming Pool Dataset [51]					Urban Tree Crown Detection [66]				
	Object Size			Referring		Object Size			Referring		Object Size			Referring	
	Small	Medium	Large	Single	Multi	Small	Medium	Large	Single	Multi	Small	Medium	Large	Single	Multi
GeoChat [26]	2.5	3.2	14.7	13.2	1.9	0.0	3.1	7.3	1.2	0.6	0.0	1.8	8.9	2.9	3.1
InternVL2-4B [12]	7.1	12.7	25.5	23.0	8.1	0.6	6.6	8.9	4.5	0.9	0.0	3.2	13.4	5.9	3.1
InternVL2-8B [12]	4.3	11.8	20.7	21.7	5.9	0.3	4.7	18.3	7.6	0.5	0.6	4.0	17.1	7.9	3.9
EarthDial [51]	11.7	14.2	23.1	25.4	8.9	1.0	7.4	24.9	8.4	1.0	1.1	7.0	25.7	11.1	6.7
Ours	15.4	23.4	37.9	30.7	14.4	1.8	10.1	33.9	11.0	1.9	0.0	5.8	22.9	8.2	8.0



Fig. 4: Qualitative comparison for visual grounding. These instances correspond to the quantitative results from Tab. 1. For each sample, we provide predictions by our approach in green, InternVL [12] in orange, and EarthDial [51] in yellow. The ground truth bounding boxes are shown in red.

Swimming Pool [51], and UCAS-AOD [76]. These datasets cover diverse object categories and data types ranging from standard imagery to thermal data.

Task. Grounding description is a challenging task, where the model predicts both a natural language response \mathbf{a} and corresponding bounding box locations ℓ . This dual-output structure requires an integrated capacity for both high-level linguistic reasoning and precise localization. We evaluate localization accuracy

Table 3: Quantitative results for zero-shot grounding description. We evaluate our model’s ability to generate both textual descriptions and corresponding bounding boxes for given text queries and images. Performance is reported with ROUGE-1 (R-1), ROUGE-L (R-L), METEOR (M-T) scores, and accuracy (%) for bounding box prediction (IoU > 0.5 and 0.25).

Model	HIT-UAV [53]					NWPU VHR-10 [14]					Swimming Pool Dataset [51]					UCAS-AOD [76]				
	@0.5	@0.25	R-1	R-L	MT	@0.5	@0.25	R-1	R-L	MT	@0.5	@0.25	R-1	R-L	MT	@0.5	@0.25	R-1	R-L	MT
GPT-4o	0.1	0.7	14.2	10.6	7.2	0.7	6.1	14.7	10.8	9.4	0.1	1.2	12.9	10.1	7.8	0.1	1.3	14.7	11.1	6.0
InternVL2-4B [12]	0.6	6.4	28.1	27.7	24.0	10.6	29.9	30.7	29.1	21.9	0.8	4.2	28.3	28.1	24.6	4.6	31.8	21.0	20.0	11.6
GeoChat [26]	0.8	8.0	22.8	22.2	22.3	2.2	15.3	21.5	20.7	21.4	1.8	8.8	21.4	21.1	24.0	1.4	13.6	20.0	18.8	14.2
EarthDial [51]	2.6	13.9	28.3	28.1	22.2	17.1	41.0	27.0	26.3	23.1	1.9	7.4	29.7	29.3	22.8	8.5	34.0	21.2	20.3	13.0
Ours	3.4	14.1	30.5	29.8	22.5	21.3	40.1	35.4	33.5	26.4	1.2	7.3	32.1	30.8	25.1	3.3	21.1	33.2	30.9	15.2

at IoU thresholds of 0.5 and 0.25 (Acc@0.5 and Acc@0.25), and assess the text quality using ROUGE-1 (R-1), ROUGE-L (R-L), and METEOR (MT) scores.

Discussion. We provide quantitative comparisons for zero-shot grounding description in Tab. 3. Our model achieves the most consistent performance overall, while outperforming the baseline approaches on ROUGE text metrics (R-1 and R-L) across all four benchmarks. This improvement is particularly notable on UCAS-AOD, where our model achieves a 33.2% R-1 score, a +12.0% absolute gain over the best baseline EarthDial. Furthermore, our method demonstrates strong localization capabilities, surpassing EarthDial by +4.2% in Acc@0.5 on the NWPU VHR-10 dataset.

4.3 Visual question answering

Datasets. We evaluate the performance of our method on visual question answering (VQA) for remote sensing using the HRBEN and LRBEN benchmarks [36]. Both datasets focus on answering questions about the content of aerial images. On HRBEN, we provide comparisons on the default test set of 62,554 question-answer pairs in a zero-shot manner. We additionally evaluate on the LRBEN test set to provide a comprehensive comparison against existing baselines.

Tasks. We consider two question types (presence, comparison) for HRBEN and three types (presence, comparison, rural/urban classification) for LRBEN, in alignment with prior work [23, 26, 39]. The goal of presence questions is classifying whether a specific instance is part of an image (e.g., “Is there a grass area on the right of a commercial building?”). Comparison questions require estimating and contrasting two quantities (e.g., “Are there more water areas than commercial buildings?” or “Is the number of buildings equal to the number of roads?”). While presence questions primarily rely on object detection, comparison questions involve both object detection and numerical reasoning, making them inherently more challenging. Rural/urban classification predicts whether an area is urban or rural based on visual criteria such as building density, thus involving scene-level classification rather than object detection.

Discussion. In Tab. 4, we provide quantitative comparisons for both HRBEN and LRBEN. Our method achieves the best overall zero-shot generalization performance on HRBEN. While LRBEN is fairly saturated and the gap to EarthDial [51] is small (−0.4% average accuracy), our method successfully sets a new

Table 4: Quantitative VQA results. The columns report the accuracy for Presence, Comparison, and Rural/Urban question types, along with the average scores.

(a) Results on HRBEN.				(b) Results on LRBEN.			
Model	Pres.	Comp.	Avg.	Model	Pres.	Comp.	R/U Avg.
Qwen-VL [5]	66.4	60.4	63.1	Qwen-VL [5]	38.6	67.6	61.0 55.4
LLaVA-1.5 [33]	69.8	67.3	68.4	LLaVA-1.5 [33]	55.5	68.2	59.0 62.8
MiniGPTv2 [10]	40.8	50.9	46.5	MiniGPTv2 [10]	55.2	55.5	39.0 55.0
GeoChat [26]	58.5	83.2	72.3	LHRS-Bot [39]	88.5	90.0	89.1 89.4
EarthGPT [73]	62.8	79.5	72.1	GeoChat [26]	91.1	90.3	94.0 90.7
EarthDial [51]	58.9	83.1	72.4	EarthDial [51]	92.6	92.7	94.0 92.7
Ours	59.4	82.7	72.5	Ours	92.2	92.5	91.0 92.3

state-of-the-art on HRBEN. Ultimately, our approach maintains highly competitive, robust performance across all question types and dataset resolutions. Crucially, this demonstrates that integrating our explicit geometric modeling to enhance spatial localization does not degrade the fundamental reasoning and question-answering capabilities of the vision-language backbone.

4.4 Ablation study

In Sec. 3.2, we introduce our dual visual grounding module, combining next-token prediction and bounding box detection. Here, we assess the impact of key components on the overall performance, see Tab. 5 for a summary.

Two token design. We compare our two-token design to a setup where we do not use the $\langle bb \rangle$ token, and instead merge both responsibilities (predicting bounding boxes in the response, producing bounding box coordinates) into a single $\langle loc \rangle$ token. As shown in Tab. 5(a), merging these tasks significantly degrades performance (29.7% vs. 33.3%), since a single embedding vector struggles to represent both the text meaning and the precise geometric coordinates.

Hungarian matching. We further investigate the role of the Hungarian algorithm in bounding box regression. As shown in Tab. 5(a), applying a global class-agnostic matching scheme (\checkmark_{glb}) provides marginal improvement over disabling matching entirely (31.2% vs. 31.0%). In contrast, our expression-grouped matching defined in Eq. (7) boosts overall performance to 33.3%. This underscores that global assignments struggle to resolve spatial ambiguities, particularly for the grounding task where 95.5% of the samples contain multiple objects.

Loss weight. We explore the effect of different values for λ_{bb} , which specifies the weight of the grounding loss $\mathcal{L}_{\text{ground}}$ defined in Eq. (6). We find that setting $\lambda_{bb} = 10$ yields the best overall performance, as shown in Tab. 5(b).

Orientation sensitivity. To quantify the importance of oriented bounding boxes, we compare our fully oriented predictions against two baselines: (i) training with oriented boxes but ignoring the predicted angle at evaluation time, and (ii) training and evaluating with standard axis-aligned boxes. As shown in Tab. 5(c), the fully oriented approach yields a substantial +5.0% overall improvement over the axis-aligned variant, with the most pronounced gains on large

Table 5: Ablation study. (a) We assess the impact of removing the Hungarian matching, and evaluate how our two-token design compares to merging both tasks into a single token. We further compare our expression-grouped matching defined in Eq. (7) to global Hungarian matching (\checkmark_{glb}). (b) We quantify the impact of the loss weight λ_{bb} on visual grounding accuracy. (c) We compare using oriented bounding boxes against dropping the angle at evaluation time, and against training and evaluating with axis-aligned boxes. (d) Moreover, we compare our sigmoid-constrained output with standard ℓ_1 loss against an unconstrained linear output and a circular ℓ_1 loss for angle periodicity.

(a) Matching		(b) Weight	(c) Orientation		(d) Grounding							
Hung.	$\langle bb \rangle$	λ_{bb}	Train w/	Eval w/	Loss	w/ Sigmoid	Small	Medium	Large	Grounding	Referring	Overall
	\checkmark	10	\checkmark	\checkmark	\mathcal{L}_1	\checkmark	11.4	37.7	54.3	28.6	31.2	31.0
\checkmark		10	\checkmark	\checkmark	\mathcal{L}_1	\checkmark	10.8	35.7	53.1	26.8	29.9	29.7
\checkmark_{glb}	\checkmark	10	\checkmark	\checkmark	\mathcal{L}_1	\checkmark	12.3	37.0	55.1	28.2	31.5	31.2
\checkmark	\checkmark	5	\checkmark	\checkmark	\mathcal{L}_1	\checkmark	13.0	39.2	56.4	30.7	32.8	32.7
\checkmark	\checkmark	20	\checkmark	\checkmark	\mathcal{L}_1	\checkmark	12.9	40.3	55.8	30.7	33.2	33.0
\checkmark	\checkmark	10	\checkmark		\mathcal{L}_1	\checkmark	11.8	33.3	40.8	24.8	26.8	26.7
\checkmark	\checkmark	10			\mathcal{L}_1	\checkmark	13.4	36.1	40.0	25.7	28.5	28.3
\checkmark	\checkmark	10	\checkmark	\checkmark	\mathcal{L}_1		11.8	36.8	55.6	30.4	31.1	31.0
\checkmark	\checkmark	10	\checkmark	\checkmark	Circ. \mathcal{L}_1	\checkmark	12.7	35.0	39.5	24.5	27.7	27.5
\checkmark	\checkmark	10	\checkmark	\checkmark	\mathcal{L}_1	\checkmark	13.5	39.5	57.9	30.9	33.4	33.3

objects (+17.9%). This confirms that explicit orientation modeling is essential for remote sensing, where objects frequently appear at arbitrary slanted angles. **Loss function and periodicity.** In Tab. 5(d), we ablate the grounding head design. Removing the sigmoid constraint for an unconstrained linear head drops performance to 31.0%. We also test a circular ℓ_1 loss to handle $0^\circ/180^\circ$ angular periodicity, formulated as $\mathcal{L}_{\text{circ}} = \min(|d| \bmod 1, 1 - (|d| \bmod 1))$, where d is the normalized angle difference. However, this further decreases performance to 27.5%. This suggests that topological boundary cases are sufficiently rare in our dataset, and that the convex stability of the standard ℓ_1 loss heavily outweighs the theoretical benefits of strict angular periodicity.

5 Conclusion

We present *SATGround*, a novel approach for spatially-aware visual grounding in remote sensing. Our method integrates multi-modal learning with a specialized localization mechanism, enabling precise alignment of textual queries with visual semantics in satellite imagery. By finetuning a generalist vision-language model with specialized control tokens and a custom grounding module, we bridge the gap between language and spatial reasoning. Our experiments demonstrate that our model outperforms existing techniques across multiple benchmarks, including referring expression detection, grounding description, and visual question answering. Notably, we achieve a significant 33.2% relative improvement in visual grounding accuracy over prior methods, underscoring the effectiveness of our structured localization approach for real-world satellite data analysis.

References

1. Achiam, J., Adler, S., Agarwal, S., Ahmad, L., Akkaya, I., Aleman, F.L., Almeida, D., Altenschmidt, J., Altman, S., Anadkat, S., et al.: Gpt-4 technical report. arXiv:2303.08774 (2023)
2. Abdin et al., M.: Phi-3 technical report: A highly capable language model locally on your phone. Tech. rep. (August 2024)
3. Alexandridis, K.P., Elezi, I., Deng, J., Nguyen, A., Luo, S.: Fractal calibration for long-tailed object detection. In: CVPR (2025)
4. Aschbacher, J.: Esa’s earth observation strategy and copernicus. Satellite earth observations and their impact on society and policy (2017)
5. Bai, J., Bai, S., Yang, S., Wang, S., Tan, S., Wang, P., Lin, J., Zhou, C., Zhou, J.: Qwen-vl: A frontier large vision-language model with versatile abilities. arXiv:2308.12966 (2023)
6. Bazi, Y., Al Rahhal, M.M., Mekhalfi, M.L., Al Zuair, M.A., Melgani, F.: Bi-modal transformer-based approach for visual question answering in remote sensing imagery. IEEE Transactions on Geoscience and Remote Sensing (2022)
7. Carion, N., Massa, F., Synnaeve, G., Usunier, N., Kirillov, A., Zagoruyko, S.: End-to-end object detection with transformers. In: ECCV (2020)
8. Changpinyo, S., Sharma, P., Ding, N., Soricut, R.: Conceptual 12m: Pushing web-scale image-text pre-training to recognize long-tail visual concepts. In: CVPR (2021)
9. Chappuis, C., Zermatten, V., Lobry, S., Le Saux, B., Tuia, D.: Prompt-rsvqa: Prompting visual context to a language model for remote sensing visual question answering. In: CVPR (2022)
10. Chen, J., Zhu, D., Shen, X., Li, X., Liu, Z., Zhang, P., Krishnamoorthi, R., Chandra, V., Xiong, Y., Elhoseiny, M.: Minigpt-v2: large language model as a unified interface for vision-language multi-task learning. arXiv:2310.09478 (2024)
11. Chen, K., Zhang, Z., Zeng, W., Zhang, R., Zhu, F., Zhao, R.: Shikra: Unleashing multimodal llm’s referential dialogue magic. arXiv:2306.15195 (2023)
12. Chen, Z., Wu, J., Wang, W., Su, W., Chen, G., Xing, S., Zhong, M., Zhang, Q., Zhu, X., Lu, L., et al.: Internvl: Scaling up vision foundation models and aligning for generic visual-linguistic tasks. In: CVPR (2024)
13. Cheng, G., Han, J., Lu, X.: Remote sensing image scene classification: Benchmark and state of the art. Proceedings of the IEEE (2017)
14. Cheng, G., Han, J., Zhou, P., Guo, L.: Multi-class geospatial object detection and geographic image classification based on collection of part detectors. ISPRS Journal of Photogrammetry and Remote Sensing **98**, 119–132 (2014)
15. Chiang, W.L., Li, Z., Lin, Z., Sheng, Y., Wu, Z., Zhang, H., Zheng, L., Zhuang, S., Zhuang, Y., Gonzalez, J.E., et al.: Vicuna: An open-source chatbot impressing gpt-4 with 90%* chatgpt quality. See <https://vicuna.lmsys.org> (accessed 14 April 2023) (2023)
16. Du, Y., Wei, F., Zhang, Z., Shi, M., Gao, Y., Li, G.: Learning to prompt for open-vocabulary object detection with vision-language model. In: CVPR (2022)
17. Elezi, I., Seidenschwarz, J., Wagner, L., Vascon, S., Torcinovich, A., Pelillo, M., Leal-Taixé, L.: The group loss $^{++}$: A deeper look into group loss for deep metric learning. tPAMI (2023)
18. Fomenko, V., Elezi, I., Ramanan, D., Leal-Taixé, L., Osep, A.: Learning to discover and detect objects. In: NeurIPS (2022)

19. Goktepe, M., hossein Shamseddin, A., Uysal, E., Monteagudo, J.M., Drees, L., Toker, A., Asseng, S., von Bloh, M.: Ecomapper: Generative modeling for climate-aware satellite imagery. In: Forty-second International Conference on Machine Learning (2025)
20. Gu, X., Lin, T.Y., Kuo, W., Cui, Y.: Open-vocabulary object detection via vision and language knowledge distillation. ICLR (2022)
21. Gupta, R., Goodman, B., Patel, N., Hosfelt, R., Sajeev, S., Heim, E., Doshi, J., Lucas, K., Choset, H., Gaston, M.: Creating xbd: A dataset for assessing building damage from satellite imagery. In: CVPRW (2019)
22. Hu, E.J., Shen, Y., Wallis, P., Allen-Zhu, Z., Li, Y., Wang, S., Wang, L., Chen, W., et al.: Lora: Low-rank adaptation of large language models. In: ICLR (2022)
23. Hu, Y., Yuan, J., Wen, C., Lu, X., Li, X.: Rsgpt: A remote sensing vision language model and benchmark. arXiv:2307.15266 (2023)
24. Irvin, J.A., Liu, E.R., Chen, J.C., Dormoy, I., Kim, J., Khanna, S., Zheng, Z., Ermon, S.: Teochat: A large vision-language assistant for temporal earth observation data. In: ICLR (2025)
25. Jia, C., Yang, Y., Xia, Y., Chen, Y.T., Parekh, Z., Pham, H., Le, Q., Sung, Y.H., Li, Z., Duerig, T.: Scaling up visual and vision-language representation learning with noisy text supervision. In: ICML (2021)
26. Kuckreja, K., Danish, M.S., Naseer, M., Das, A., Khan, S., Khan, F.S.: Geochat: Grounded large vision-language model for remote sensing. In: CVPR (2024)
27. Kuhn, H.W.: The hungarian method for the assignment problem. *Naval research logistics quarterly* (1955)
28. Lai, X., Tian, Z., Chen, Y., Li, Y., Yuan, Y., Liu, S., Jia, J.: Lisa: Reasoning segmentation via large language model. In: CVPR (2024)
29. Li, L.H., Zhang, P., Zhang, H., Yang, J., Li, C., Zhong, Y., Wang, L., Yuan, L., Zhang, L., Hwang, J.N., et al.: Grounded language-image pre-training. In: CVPR (2022)
30. Li, X., Wen, C., Hu, Y., Yuan, Z., Zhu, X.X.: Vision-language models in remote sensing: Current progress and future trends. *IEEE Geoscience and Remote Sensing Magazine* (2024)
31. Li, X., Wen, C., Hu, Y., Zhou, N.: Rs-clip: Zero shot remote sensing scene classification via contrastive vision-language supervision. *International Journal of Applied Earth Observation and Geoinformation* (2023)
32. Lin, T.Y., Maire, M., Belongie, S., Hays, J., Perona, P., Ramanan, D., Dollár, P., Zitnick, C.L.: Microsoft coco: Common objects in context. In: ECCV (2014)
33. Liu, H., Li, C., Li, Y., Lee, Y.J.: Improved baselines with visual instruction tuning. In: CVPR (2024)
34. Liu, H., Li, C., Wu, Q., Lee, Y.J.: Visual instruction tuning. In: NeurIPS (2024)
35. Liu, S., Cheng, H., Liu, H., Zhang, H., Li, F., Ren, T., Zou, X., Yang, J., Su, H., Zhu, J., et al.: Llava-plus: Learning to use tools for creating multimodal agents. In: ECCV (2024)
36. Lobry, S., Marcos, D., Murray, J., Tuia, D.: Rsvqa: Visual question answering for remote sensing data. *IEEE Transactions on Geoscience and Remote Sensing* (2020)
37. Lu, J., Batra, D., Parikh, D., Lee, S.: Vilbert: Pretraining task-agnostic visiolinguistic representations for vision-and-language tasks. *NeurIPS* **32** (2019)
38. Minderer, M., Gritsenko, A., Stone, A., Neumann, M., Weissenborn, D., Dosovitskiy, A., Mahendran, A., Arnab, A., Dehghani, M., Shen, Z., et al.: Simple open-vocabulary object detection. In: ECCV (2022)
39. Muhtar, D., Li, Z., Gu, F., Zhang, X., Xiao, P.: Lhrs-bot: Empowering remote sensing with vgi-enhanced large multimodal language model. In: ECCV (2024)

40. Pang, C., Wu, J., Li, J., Liu, Y., Sun, J., Li, W., Weng, X., Wang, S., Feng, L., Xia, G.S., et al.: H2rsvlm: Towards helpful and honest remote sensing large vision language model. *CoRR* (2024)
41. Peng, B., Li, C., He, P., Galley, M., Gao, J.: Instruction tuning with gpt-4. *arXiv:2304.03277* (2023)
42. Peng, Z., Wang, W., Dong, L., Hao, Y., Huang, S., Ma, S., Ye, Q., Wei, F.: Grounding multimodal large language models to the world. In: *ICLR* (2024)
43. Plummer, B.A., Wang, L., Cervantes, C.M., Caicedo, J.C., Hockenmaier, J., Lazebnik, S.: Flickr30k entities: Collecting region-to-phrase correspondences for richer image-to-sentence models. In: *ICCV* (2015)
44. Qiu, C., Yu, A., Yi, X., Guan, N., Shi, D., Tong, X.: Open self-supervised features for remote-sensing image scene classification using very few samples. *IEEE Geoscience and Remote Sensing Letters* (2022)
45. Radford, A., Kim, J.W., Hallacy, C., Ramesh, A., Goh, G., Agarwal, S., Sastry, G., Askell, A., Mishkin, P., Clark, J., et al.: Learning transferable visual models from natural language supervision. In: *ICML* (2021)
46. Rahnmooonfar, M., Chowdhury, T., Sarkar, A., Varshney, D., Yari, M., Murphy, R.R.: Floodnet: A high resolution aerial imagery dataset for post flood scene understanding. *IEEE Access* (2021)
47. Schuhmann, C., Beaumont, R., Vencu, R., Gordon, C., Wightman, R., Cherti, M., Coombes, T., Katta, A., Mullis, C., Wortsman, M., et al.: Laion-5b: An open large-scale dataset for training next generation image-text models. In: *NeurIPS* (2022)
48. Schwartz, E., Choshen, L., Shtok, J., Doveh, S., Karlinsky, L., Arbel, A.: Numerologic: Number encoding for enhanced llms' numerical reasoning. In: *EMNLP* (2024)
49. Shen, R., Bubeck, S., Eldan, R., Lee, Y.T., Li, Y., Zhang, Y.: Positional description matters for transformers arithmetic. *arXiv:2311.14737* (2023)
50. Singh, A.K., Strouse, D.: Tokenization counts: the impact of tokenization on arithmetic in frontier llms. *arXiv:2402.14903* (2024)
51. Soni, S., Dudhane, A., Debary, H., Fiaz, M., Munir, M.A., Danish, M.S., Fraccaro, P., Watson, C.D., Klein, L.J., Khan, F.S., Khan, S.: Earthdial: Turning multi-sensory earth observations to interactive dialogues. In: *CVPR* (2025)
52. Stewart, R., Andriluka, M., Ng, A.Y.: End-to-end people detection in crowded scenes. In: *CVPR* (2016)
53. Suo, J., Wang, T., Zhang, X., Chen, H., Zhou, W., Shi, W.: Hit-uav: A high-altitude infrared thermal dataset for unmanned aerial vehicle-based object detection. *Scientific Data* **10**(1), 227 (2023)
54. Taori, R., Gulrajani, I., Zhang, T., Dubois, Y., Li, X., Guestrin, C., Liang, P., Hashimoto, T.B.: Stanford alpaca: an instruction-following llama model (2023). URL https://github.com/tatsu-lab/stanford_alpaca **1**(9) (2023)
55. Toker, A., Eisenberger, M., Cremers, D., Leal-Taix'e, L.: Satsynth: Augmenting image-mask pairs through diffusion models for aerial semantic segmentation. 2024 *IEEE/CVF Conference on Computer Vision and Pattern Recognition (CVPR)* (2024)
56. Toker, A., Kondmann, L., Weber, M., Eisenberger, M., Camero, A., Hu, J., Hoderlein, A.P., Senaras, C., Davis, T., Cremers, D., Marchisio, G., Zhu, X., Leal-Taixe, L.: Dynamicearthnet: Daily multi-spectral satellite dataset for semantic change segmentation. In: *Proceedings of the IEEE/CVF Conference on Computer Vision and Pattern Recognition (CVPR)* (2022)

57. Toker, A., Zhou, Q., Maximov, M., Leal-Taixe, L.: Coming down to earth: Satellite-to-street view synthesis for geo-localization. In: Proceedings of the IEEE/CVF Conference on Computer Vision and Pattern Recognition (CVPR) (2021)
58. Touvron, H., Lavril, T., Izacard, G., Martinet, X., Lachaux, M.A., Lacroix, T., Rozière, B., Goyal, N., Hambro, E., Azhar, F., et al.: Llama: Open and efficient foundation language models. arXiv:2302.13971 (2023)
59. Wang, W., Lv, Q., Yu, W., Hong, W., Qi, J., Wang, Y., Ji, J., Yang, Z., Zhao, L., XiXuan, S., Xu, J., Chen, K., Xu, B., Li, J., Dong, Y., Ding, M., Tang, J.: CogVLM: Visual expert for pretrained language models. In: NeurIPS (2024)
60. Woodcock, C.E., Allen, R., Anderson, M., Belward, A., Bindschadler, R., Cohen, W., Gao, F., Goward, S.N., Helder, D., Helmer, E., et al.: Free access to landsat imagery. *Science* (2008)
61. Xu, M., Zhang, Z., Wei, F., Lin, Y., Cao, Y., Hu, H., Bai, X.: A simple baseline for open-vocabulary semantic segmentation with pre-trained vision-language model. In: ECCV (2022)
62. Yao, L., Huang, R., Hou, L., Lu, G., Niu, M., Xu, H., Liang, X., Li, Z., Jiang, X., Xu, C.: FILIP: Fine-grained interactive language-image pre-training. In: ICLR (2022)
63. You, H., Zhang, H., Gan, Z., Du, X., Zhang, B., Wang, Z., Cao, L., Chang, S.F., Yang, Y.: Ferret: Refer and ground anything anywhere at any granularity. In: ICLR (2024)
64. Yuan, L., Chen, D., Chen, Y.L., Codella, N., Dai, X., Gao, J., Hu, H., Huang, X., Li, B., Li, C., et al.: Florence: A new foundation model for computer vision. arXiv:2111.11432 (2021)
65. Yuan, Z., Mou, L., Wang, Q., Zhu, X.X.: From easy to hard: Learning language-guided curriculum for visual question answering on remote sensing data. *IEEE transactions on geoscience and remote sensing* (2022)
66. Zamboni, P., Junior, J.M., Silva, J.d.A., Miyoshi, G.T., Matsubara, E.T., Nogueira, K., Gonçalves, W.N.: Benchmarking anchor-based and anchor-free state-of-the-art deep learning methods for individual tree detection in rgb high-resolution images. *Remote Sensing* (2021)
67. Zhai, X., Mustafa, B., Kolesnikov, A., Beyer, L.: Sigmoid loss for language image pre-training. In: ICCV (2023)
68. Zhan, Y., Xiong, Z., Yuan, Y.: Skyeyegpt: Unifying remote sensing vision-language tasks via instruction tuning with large language model. *ISPRS Journal of Photogrammetry and Remote Sensing* (2025)
69. Zhang, H., Li, F., Liu, S., Zhang, L., Su, H., Zhu, J., Ni, L., Shum, H.Y.: DINO: DETR with improved denoising anchor boxes for end-to-end object detection. In: ICLR (2023)
70. Zhang, H., Li, H., Li, F., Ren, T., Zou, X., Liu, S., Huang, S., Gao, J., Leizhang, Li, C., et al.: Llava-grounding: Grounded visual chat with large multimodal models. In: ECCV (2024)
71. Zhang, J., Huang, J., Jin, S., Lu, S.: Vision-language models for vision tasks: A survey. *IEEE Transactions on Pattern Analysis and Machine Intelligence* (2024)
72. Zhang, R., Guo, Z., Zhang, W., Li, K., Miao, X., Cui, B., Qiao, Y., Gao, P., Li, H.: Pointclip: Point cloud understanding by clip. In: CVPR (2022)
73. Zhang, W., Cai, M., Zhang, T., Zhuang, Y., Mao, X.: Earthgpt: A universal multimodal large language model for multisensor image comprehension in remote sensing domain. *IEEE Transactions on Geoscience and Remote Sensing* (2024)
74. Zhao, Y., Lin, Z., Zhou, D., Huang, Z., Feng, J., Kang, B.: Bubogpt: Enabling visual grounding in multi-modal llms. arXiv:2307.08581 (2023)

75. Zhu, D., Chen, J., Shen, X., Li, X., Elhoseiny, M.: MiniGPT-4: Enhancing vision-language understanding with advanced large language models. In: ICLR (2024)
76. Zhu, H., Chen, X., Dai, W., Fu, K., Ye, Q., Jiao, J.: Orientation robust object detection in aerial images using deep convolutional neural network. In: ICIP (2015)
77. Zhu, X., Zhang, R., He, B., Guo, Z., Zeng, Z., Qin, Z., Zhang, S., Gao, P.: Pointclip v2: Prompting clip and gpt for powerful 3d open-world learning. In: ICCV (2023)
78. Zia, U., Riaz, M.M., Ghafoor, A.: Transforming remote sensing images to textual descriptions. International Journal of Applied Earth Observation and Geoinformation (2022)